

Article

Study of the Effect of External Magnetic Fields on the Parameters of the Electrical Communications Probing System for a Microtunneling Shield

Andrew Zhivodernikov, Alexander Pavlenko *, Artem Khoroshev and Vladimir Puzin

Research Institute of Electromechanics, Platov South-Russian State Polytechnic University (NPI),
Prosveshcheniya str., 132, 346428 Novocherkassk, Russia

* Correspondence: eea.srspu@gmail.com; Tel.: +7-8635255473

Abstract: The issues were reviewed in assessing external electromagnetic fields' effect on the parameters of an electrical power line probing system based on three-component ferroprobes for detecting active underground power cable lines during microtunnel construction using the thrust boring method (by tunneling shield) in densely populated urban areas. A study was conducted on the change in the topology of the energized cable magnetic field located in the external magnetic field area created by operating electrical equipment under the influence of an external electromagnetic field and a tunneling shield with installed magneto-sensitive detectors. Experimental studies of the probing system were made. Options have been proposed for compensating the inductance component of the external magnetic field during tunnel driving in urban development and industrial area conditions.

Keywords: microtunneling shield; underground power line; external electromagnetic field; advanced probing system; magnetic sensor

Citation: Zhivodernikov, A.; Pavlenko, A.; Khoroshev, A.; Puzin, V. Study of the Effect of External Magnetic Fields on the Parameters of the Electrical Communications Probing System for a Microtunneling Shield. *Inventions* **2022**, *7*, 121. <https://doi.org/10.3390/inventions7040121>

Academic Editor: Chien-Hung Liu

Received: 8 November 2022

Accepted: 8 December 2022

Published: 12 December 2022

Publisher's Note: MDPI stays neutral with regard to jurisdictional claims in published maps and institutional affiliations.



Copyright: © 2022 by the authors. Licensee MDPI, Basel, Switzerland. This article is an open access article distributed under the terms and conditions of the Creative Commons Attribution (CC BY) license (<https://creativecommons.org/licenses/by/4.0/>).

1. Introduction

During tunnel boring operations, external methods of reconnaissance of the route are mainly used to detect existing underground utilities [1,2]. In urban areas, such methods are not always applicable. At the same time, the placement of probing systems directly on the tunnel boring shield is also not always possible due to the size of such systems or the destructive effect of the rock. The dimensions of microtunneling shields even only allow the use of compact sounding systems and only as part of an automated control system with sensors located in the uninhabited part of the tunneling shield (a review of sounding systems was carried out by the authors in work [3]). In the considered design of the microtunneling shield, a built-in electromagnetic system for probing underground utilities is used. The earlier work of the authors covered the issues of numerical modeling of a system for advanced probing of underground electrical communications with the placement of magneto-sensitive detectors in a tunneling shield intending to assess the possibility of such system creation [4]. At the same time, the numerical model was verified by comparing it to the results of the analytical calculation, and full-scale experiments were conducted, which served as a basis to confirm the possibility of implementing a ferroprobe-based probing system [5]. In this context, a significant effect of external electromagnetic fields was noted between the geomagnetic field, the background electromagnetic field of industrial areas, and urban development. The issues in assessing the possibility of detecting a power cable line located in a reinforced concrete tray at a 3 m distance from the end of the microtunneling shield were also reviewed [6]. At the same time, a simulation of the change in the pattern of the distribution of the magnetic field was performed depending on the relative position of the three-phase power cable line conductors.

In this paper, numerical simulation is used to assess the effect of an external magnetic field on the possibility of detecting a power cable line at a given distance when ferroprobes are used as magneto-sensitive detectors. The models were based on a single conductor with a current of 50 to 600 A, located at a 1 to 3 m distance from the axis of the conductor to the front end of the microtunneling shield where the ferroprobes were installed.

2. Formulation of the Problem

Previous works [4,5] used a computational domain with the Dirichlet boundary condition during the numerical simulation of the electromagnetic field of a power cable line. In this case, when an additional source of an external magnetic field was introduced into the calculation problem, the necessity arose to move to Neumann boundary conditions. Implementation of such boundary conditions in the GetDP environment for solving discrete numerical problems requires a transition to spherical boundaries in the computational domain. The magnetic flux density value in the case of an extended linear source of magnetic field—an energized conductor—can be found according to the Biot–Savart–Laplace law:

$$d\vec{B} = \mu_0 i d\vec{s} \times \vec{r} / (4\pi r^3) \quad (1)$$

where μ_0 is the magnetic permeability of vacuum, i is the current value, ds is the elementary conductor section and, r is the total displacement vector from the conductor section (ds) to the magnetic flux density value calculation point.

Accordingly, with a finite length of the conductor, results of the magnetic flux density calculation at a remote point will depend on the ratio of the conductor length and the value of the displacement vector r . If the length of the displacement vector r is more than 0.25–0.3 of the length of the energized conductor model, the calculated values of the magnetic flux density at a remote point will differ significantly from the case of an infinite length conductor. The need to provide for a sufficiently large length of the energized conductor section model in the computational domain with spherical boundaries requires a significant increase in its linear dimensions. At the same time, the computational domain volume increased from 400 m³; in work [4], the volume was 1150 m³ with a boundary sphere radius of 6.5 m. It is obvious that an increase in the computational domain size inevitably results in an increase in the number of finite elements in the mesh. To avoid multiple increases in the number of finite elements, the microtunneling shield model was simplified in comparison to the one used in [5], but the design of its body, together with the sensors, was not altered. The conductor model is made in the form of a cylinder with a diameter of 30 mm, crossing the entire computational domain, i.e., the beginning and end of the conductor model are determined by the computational domain boundaries. The conductor axis is parallel to the Z-axis of the computational domain coordinate system. The shield body is made in the form of a 4 m long pipe with a wall thickness of 20 mm. The pipe's outer diameter is 1.42 m. The longitudinal axis of the microtunneling shield model is parallel to the X-axis of the computational domain coordinate system. The body shell (cross-section 20 × 100 mm) of the tunneling shield has rectangular 35 × 80 mm holes (Figure 1) to allocate ferroprobes. Three-component ferroprobes are modeled as individual cores of each of the three measuring channels. The core length is 20 mm and the diameter is 3 mm. The longitudinal axes of the cores of each ferroprobe are parallel to the axes of the coordinate system of the computational domain following the measured component of the magnetic field vector.

Thus, the computational domain is limited by a sphere with a radius of 6.5 m containing an energized conductor (about 12 m long) and a tunneling shield body model with sensors (ferroprobes).

The scheme of the geometric model of the computational domain implemented in the Gmsh preprocessor (version 4.10.4, compiled from source code; C. Geuzaine and J.-F. Remacle, Belgium [7]) is shown in Figure 1.

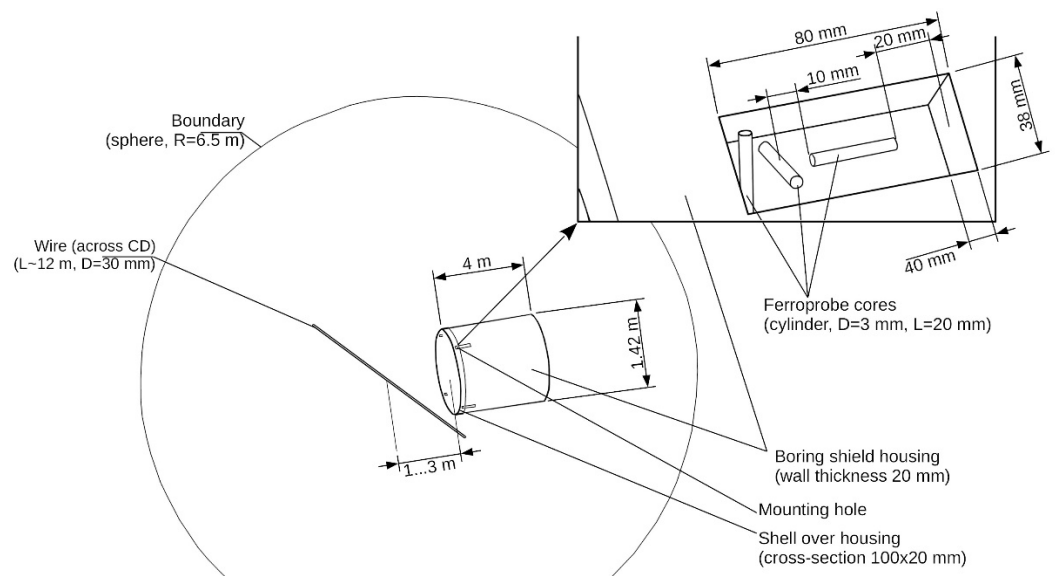


Figure 1. Geometric model of computational domain (“CD”).

The computational domain geometric model contains 110 points, 147 curves, 81 surfaces, and 16 volumes.

To build a grid, a combination of the MeshAdapt and Delaunay algorithms [8] was used, with the application of a native algorithm for optimizing the quality of grid elements (for two-dimensional and three-dimensional elements, respectively). For certain elements of the computational domain, the following characteristic lengths of finite elements were established: 700 mm for the computational domain boundary, 10 mm for the walls of the shield model, 6 mm for the conductor, and 1 mm for the ferroprobe cores.

The mesh of the finite elements of the computational domain, depending on the distance between the conductor axis and the microtunneling shield, contains 586–614 thousand nodes and 3.47–3.64 million tetrahedra.

The universal mathematical model (verified in [9]) based on the magnetic vector potential in the classical A-V formulation [10] of the electromagnetic field was used. To implement the mathematical model in the GetDP, a weak form of the A-V formulation was chosen in the form of the Galerkin equations [11,12]:

$$(v \operatorname{curl} a, \operatorname{curl} a')_{\Omega} - (j_s, a)_{\Omega_s} + (h_e, a')_{\Omega_e} + (n \times h_s, a')_{\Gamma} = 0, \quad (2)$$

where a is the magnetic vector potential, Ω is the computational domain, Ω_s is the energized conductor, Ω_e is the environment, v is the magnetic resistance, $n \times h_s$ is the boundary conditions at the boundary Γ section Ω , and h_e is the external field intensity.

The finite element method was implemented using the Gmsh + GetDP [13,14] software package and a verified implementation of the mathematical model of the electromagnetic field in a nonlinear medium based on a three-dimensional computational domain using the tree-cotree gauge condition [15–17]. In this case, for the model with the Neumann boundary conditions and an open current loop (the conductor is linear and crosses the entire computational domain), the Coulomb calibration along the boundary of the computational domain was additionally applied with the formation of the corresponding functional space of the scalar field (nodal functional space) [17]. On the boundary Γ of the computational domain, the Coulomb gauge is applied:

$$(\nabla \cdot a)_{\Gamma} = 0. \quad (3)$$

Numerical problems were solved for the values of the magnetic flux density of the external magnetic field equal to 0, 10 nT, 1 μ T, 10 μ T, and 1 mT. The magnetic field vector of the external magnetic field is directed along the Y-axis (according to the coordinate system in Figure 1). The calculation of the electromagnetic field was performed for each

value of two variables: a distance between the head of the microtunneling shield body and the axis of the conductor (wire) in the range 1–3 m with a 0.5 m step, and current values in the conductor in the range 50–600 A with a 50 A step. Accordingly, modeling was performed for 300 combinations of the computational domain parameters.

3. Computer Modeling

To solve the numerical problem, the GetDP environment (version 3.4.1, compiled from source code, P. Dular and C. Geuzaine, University of Liège, Liège, Belgium) was configured to use the PETSc toolkit (version 3.16.6, compiled from source code; Argonne National Laboratory, Lemont, IL, USA [18]) with the MUMPS solver (version 5.4.0, compiled from source code via PETSc toolkit; Mumps Technologies SAS, Lyon, France [19]). The MUMPS solver is configured to work with an alternative implementation of a set of basic subroutines for solving linear algebra problems (BLAS)—BLIS (version 3.0, compiled from source code; AMD, Santa Clara, CA, USA [20]).

The nonlinear electromagnetic problem was solved by the iterative Newton–Raphson method with an intermediate solution of the SLAE using the Cholesky method with ordering using the METIS algorithm (version 5.1.0, compiled from source code; Regents of the University of Minnesota, Minneapolis, MN, USA [21]). The order of the matrix of unknowns is $4.64\text{--}4.86 \times 10^6$, and its density is 0.00028–0.00029%. The upper limit of the error of the direct SLAE solution did not exceed 4.8×10^{-8} . The time to solve the numerical problem was 0.9–1.8 h for each option (PC with a AMD Ryzen 5 3600 processor, 64GB of RAM). Factorization was performed in out-of-core mode (up to 40 GB of RAM and up to 120 GB of disk space used). In all cases, the solution of the nonlinear problem required two to four iterations to achieve an error of less than 0.1%.

4. Modeling Results

Assessment of the effect of an external magnetic field on the distribution of the electromagnetic field of an energized conductor was performed according to two criteria: a change in the value of magnetic flux density in the region between the microtunneling shield and the cable (control line in Figure 2), as well as a change in the value of magnetic flux density in the cores of magneto-sensitive detectors (ferroprobes) in the shield body.

An external magnetic field with an induction value of over $1 \mu\text{T}$ introduces significant changes in the topology of the magnetic field of an energized conductor. The degree of the magnetic field topology change depends on the current value in the conductor: the smaller the current value, the stronger the influence of the external magnetic field. For example, let us consider the results of the electromagnetic field modeling in the computational domain with a distance of 3 m between the body of the microtunneling shield and the energized cable. The results of calculating the magnetic flux density along the control line are shown in Figure 3. An external magnetic field with an induction of 10 nT does not have a significant effect on the topology of the magnetic field of an energized cable compared to the case without an external magnetic field. An external magnetic field with an induction of $1 \mu\text{T}$ with a current value of 300 A results in a significant change in the induction along the control line at a distance of over 2.7–2.8 m from the cable axis, and with a current of 50 A, significant changes occur already at a distance of 0.8–0.9 m from the cable axis. One can also note the appearance of a local minimum of the magnetic flux density value in the immediate vicinity of the tunneling shield body end (distance 2.9 m from the cable axis). The minimum value of the magnetic flux density along the control line with an external field induction of 10 μT for a current value of 50 A is achieved at a distance of 0.9 m from the conductor, and for a current of 300 A only at 2.7 m. In this situation, the value of the local minimum is a sequence higher than for the case with a magnetic field induction of $1 \mu\text{T}$. An external field with a magnetic flux density of 1 mT results in a significant change in the topology of the energized cable electromagnetic field. Significant changes already occur at distances of 0.1–0.2 m from the axis of the energized cable and at distances of over 0.7–0.8, the value of the magnetic flux density along the

control line is almost independent from the current in the cable. Thus, an increase in current from 50 A to 300 A results in a magnetic flux density growth of 4.5% at a distance of 1 m, while at an external field flux density value of 1 μT , the change was 85%.

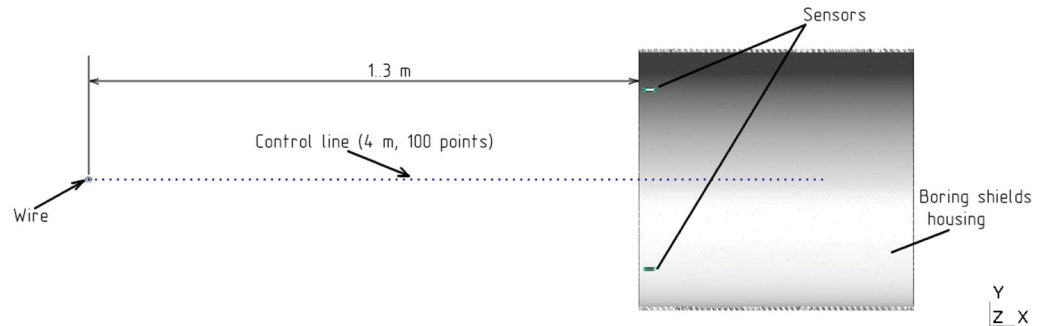


Figure 2. Location of the control line in the computational domain.

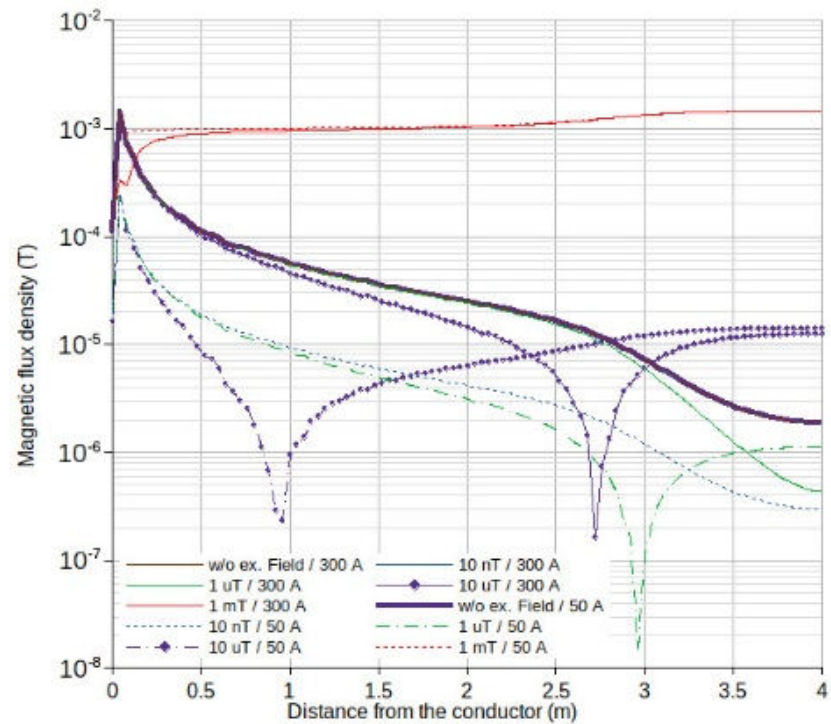


Figure 3. Values of magnetic flux density along the control line at a distance of 3 m between the microtunneling shield and the cable.

In the absence of an external magnetic field source, the values of induction in the ferroprobe cores corresponded (considering changes in the model) to the values obtained in the paper [4]. Considering the relative position of the energized cable and the microtunneling shield, the most significant changes in the magnetic flux density with a change in the cable current will be observed in the cores of the Y-components of ferropubes, which was also demonstrated in [4–6]. Figure 4 shows the dependencies of the values of the Y-component of the magnetic field vector in the core of ferroprobe No. 1 on the current value in the cable for various values of the external magnetic field induction. Figure 5 shows similar dependencies for the Z-component.

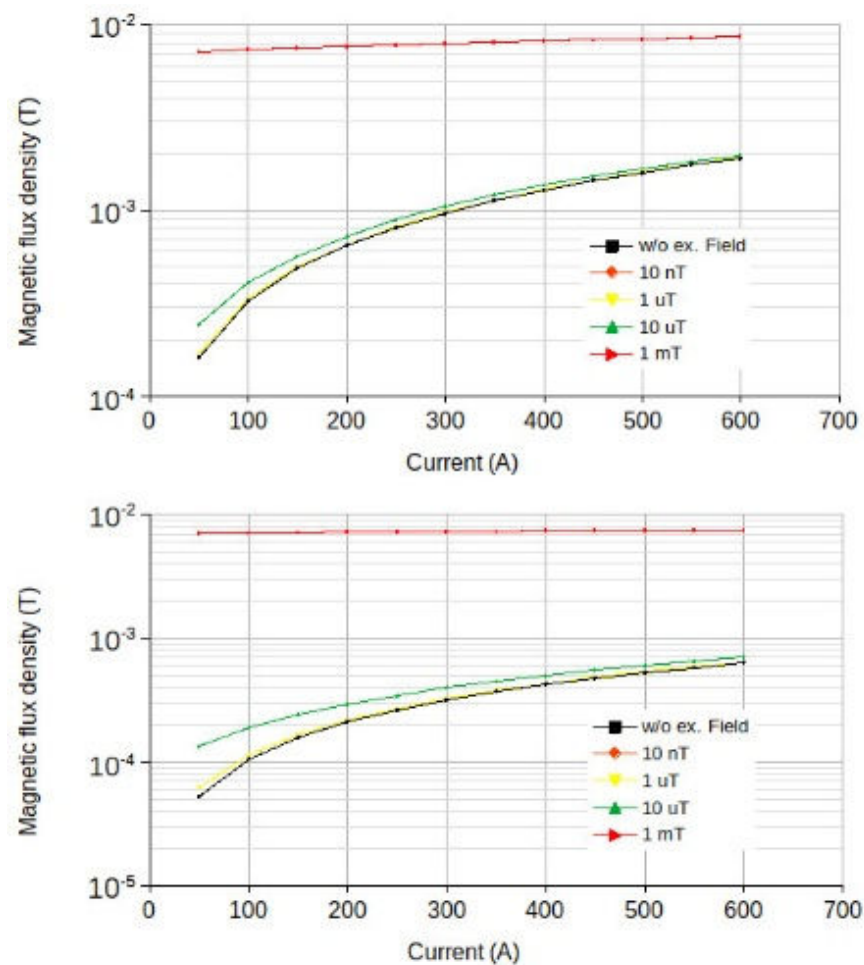


Figure 4. The dependence of the values of the Y-component of the magnetic field vector in the core of the ferroprobe on the current value in the cable for various values of the external magnetic field induction. Upper panel—distance 1 m between the microtunneling shield and the cable, lower panel—distance 3 m.

An external magnetic field with an induction of over $10 \mu\text{T}$ has a significant effect on the value of magnetic flux density in the ferroprobe cores; however, the ability of ferroprobes to detect changes in the value of magnetic flux density with a change in the current in the cable worsens insignificantly (Figure 6). The difference between the values of the Y-component of the magnetic field vector in the ferroprobe core and the current strength in the 50 A and 600 A cables without an external field and 1 m distance between the microtunneling shield and the cable axis is $1748.9 \mu\text{T}$. When exposed to an external field with an induction value of $1 \mu\text{T}$, the difference decreases to $1748.3 \mu\text{T}$, and when the magnetic flux density of the external field is $10 \mu\text{T}$, it decreases to $1743.4 \mu\text{T}$. Furthermore, only an external field with an induction value of 1 mT results in a decrease in the difference of the Y-component to $1514 \mu\text{T}$. With an increase in the distance between the microtunneling shield and the cable axis to 3 m, the difference in the values of the Y-component of the magnetic field vector in the ferroprobe core between the current strength in the cable of 50 A and 600 A in the absence of an external field, decreases to $576.6 \mu\text{T}$. An external magnetic field with an induction value of up to $10 \mu\text{T}$ does not cause a significant decrease in the difference between the values of the Y component. With an increase in the magnetic flux density value of the external field to 1 mT, the difference in the values of the Y-component decreases to $476.6 \mu\text{T}$. The nature of the change in the difference between the values of the Z-component is similar but has a trend towards an increase in the value with an increase in the value of the external field induction.

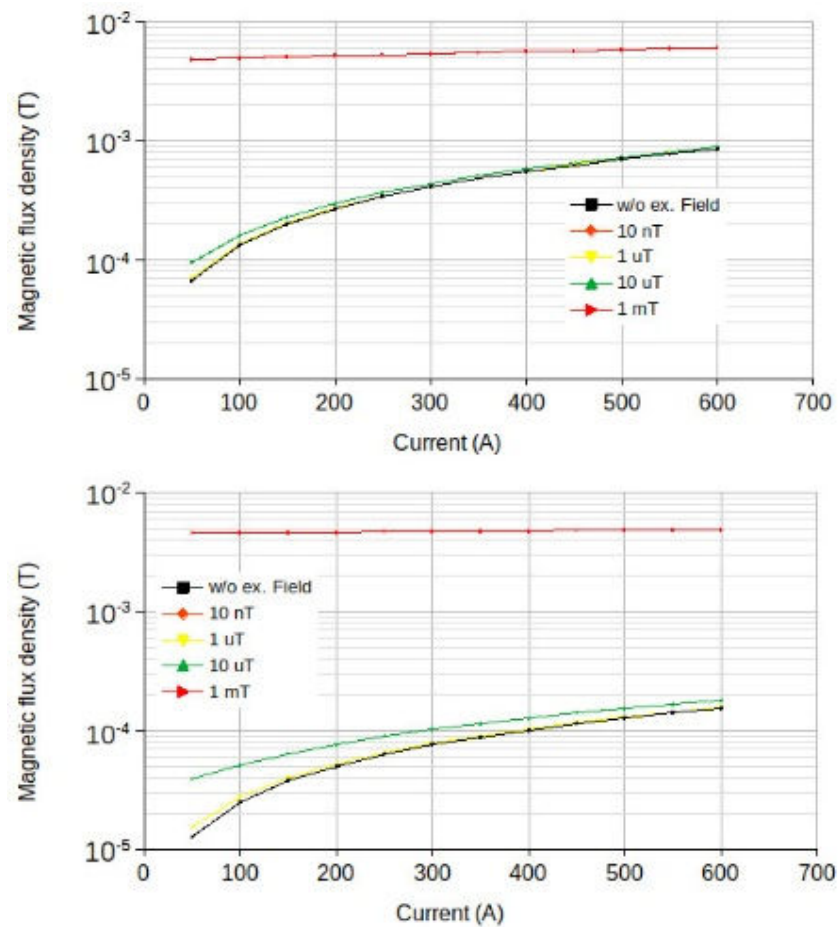


Figure 5. The dependence of the values of the magnetic field vector Z-component in the core of the ferroprobe on the current value in the cable for various values of the external magnetic field induction. Upper panel—distance 1 m between the microtunneling shield and the cable, lower panel—distance 3 m.

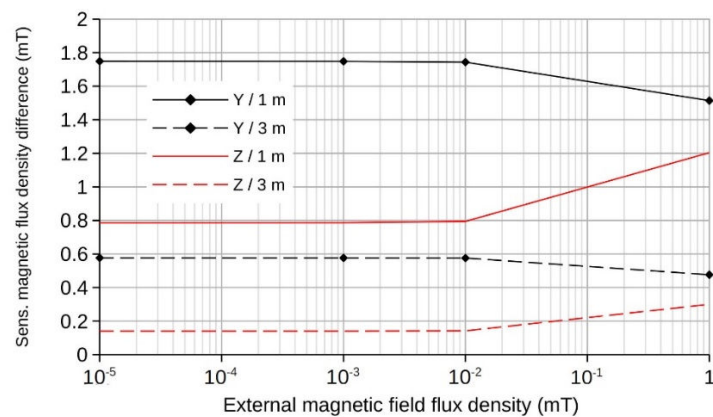


Figure 6. The dependence of the difference between the values of the Y- and Z-components of the magnetic field vector in the ferroprobe core between the current strength in the cable of 50 A and 600 A on the magnetic flux density value of the external field (for a distance of 1 and 3 m between the microtunneling shield and the cable axis).

The results show the possibility of registering the Y- and Z-components of the electromagnetic field of an energized power cable by ferroprobes in the body of a microtunneling shield at an external magnetic field induction of up to mT-sized values.

5. Assessments on the Experimental Facility

The experimental facility included a steel pipe with a diameter of 1400 mm (simulates the body of a microtunneling shield) on which four measuring modules with sensors, a power supply, an RS485-USB interface converter, and a laptop are mounted. Magnetic modulation sensors (ferroprobes) NV0391.5-35 [22] were used as sensors. For testing purposes, VbShv 3×16 (ozh)-6 power cable type was used as a probed power cable line (source of an electromagnetic field). The tested cable was placed on a cable rack at a distance of 3 m from the end of the pipe and connected to an adjustable current source. A laboratory power supply with a power of 30 kW was used as a current source. Ferroprobes placed in the mounting grooves of the pipe are equipped with bias windings for calibrating and setting the benchmark (reference) signal values at the sensor outputs. To set the benchmark (reference) values of the sensor output signals for individual measuring channels in the bias windings, current values were set at values sufficient to compensate for the effect of the constant components of external fields. The conductors of the tested cable are connected in parallel by two. At one end of the cable, the conductors are shorted to simulate a real power cable connected to a load. The current value in the cable changed in the range from 65 to 295 A. The ferroprobe was tuned to the maximum sensitivity of 200 mV/μT.

It was found that the most significant change in the signal was obtained along the Y-axis. Figure 7 shows the oscillograms of the output signals of the ferroprobe along the measuring channels (via analogue–digital converter, ADC) of the magnetic field's Y- and Z-components. One can note that the magnitude of the output signal through the Y-component channel is 2.6–2.7 times higher than through the Z-component channel, which corresponds to the results of the numerical simulation. One should note that the background external electromagnetic field has the magnitude of the Y- and Z-components of the magnetic field vector, which is two times less than the field created by the power cable at a current of 65 A (Figure 8).

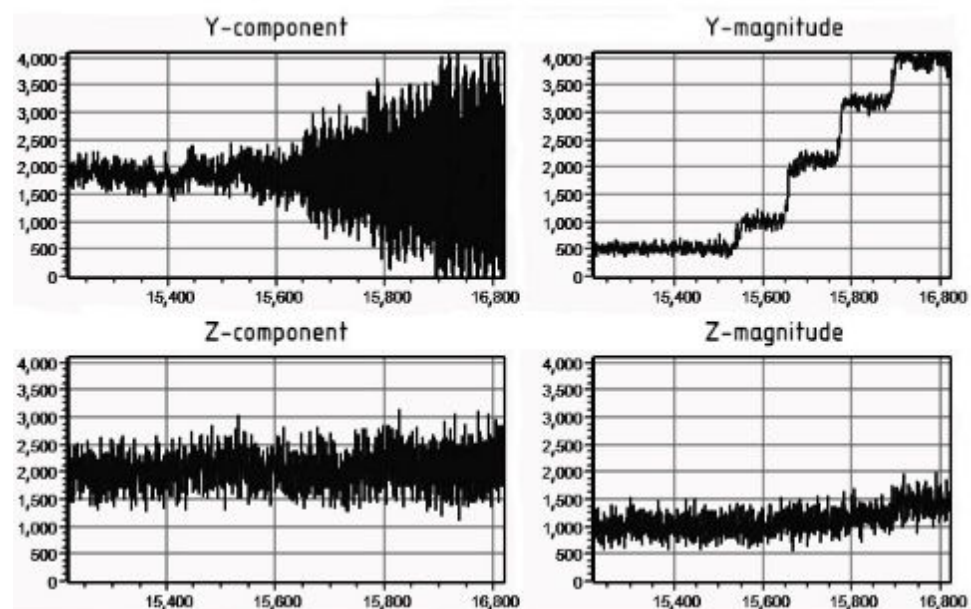


Figure 7. An oscillogram of the output signal of the ferroprobe ADC through the measuring channels of the Y- and Z-components when the current value in the cable changes from 65 to 295 A. The horizontal axis is time and the vertical axis is the conventional units of the ADC output signal level.

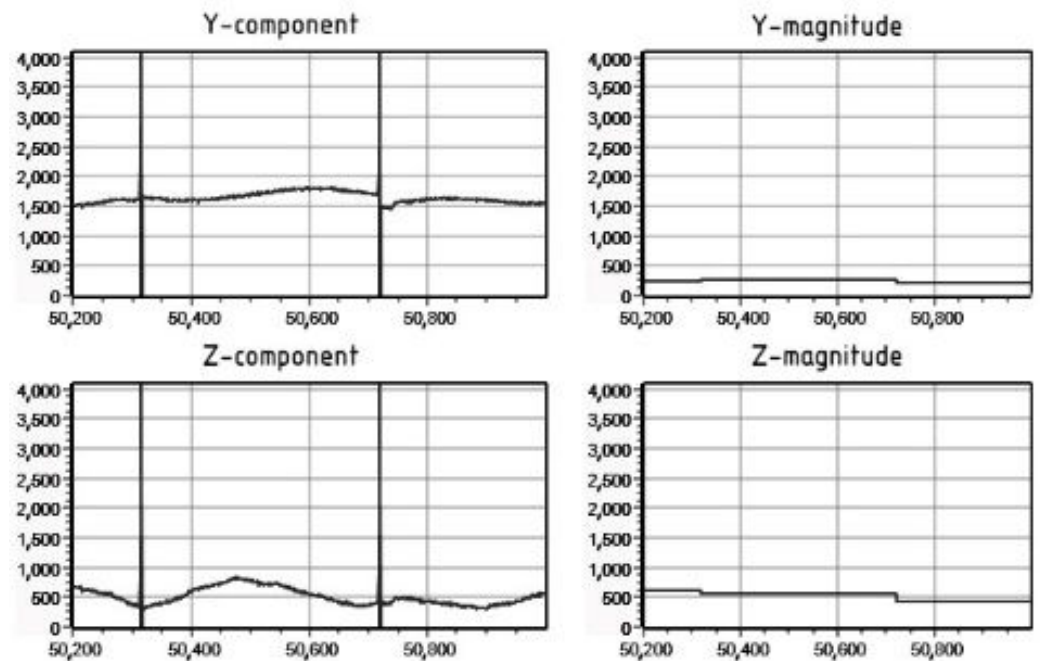


Figure 8. An oscillogram of the output signal of the ferroprobe ADC through the measuring channels of the Y- and Z-components when the cable is not energized (the background external field only). The horizontal axis is time and the vertical axis is the conventional units of the ADC output signal level.

6. Conclusions

Experiments in a qualitative manner confirm the results of the numerical simulation. When using three-component ferroprobes, the most informative is the sensor component that coincides with the direction of the magnetic field vectors of the probed power cable electromagnetic field. The use of bias windings for ferroprobes makes it possible to largely compensate for the effect of constant component of external electromagnetic fields with induction of up to 10–30 μT , which makes it possible to use these highly sensitive magnetometers when exposed to fields common for urban developments and industrial areas. However, the effect of noise caused by the inhomogeneity of external magnetic fields and the high sensitivity of ferroprobes remains significant. To mitigate the effect of these noises, additional filters will be required, especially when probing power cable lines with a current of less than 100 A. When the current values in the power cable line are over 200 amperes, it becomes possible to register signals through other measuring channels of the ferroprobe. Thus, the possibility has been confirmed of the ferroprobe operation for a microtunneling shield under the effect of external electromagnetic fields of natural and man-made origin.

Author Contributions: Conceptualization, A.Z. and A.P.; methodology, A.Z., A.K.; software, V.P.; validation, A.Z., A.K.; formal analysis, A.P.; investigation, A.K., V.P.; resources, V.P.; data curation, A.P.; writing—original draft preparation, A.Z., A.K.; writing—review and editing, A.P.; visualization, A.P.; project administration, V.P.; funding acquisition, V.P. All authors have read and agreed to the published version of the manuscript.

Funding: This research received no external funding.

Data Availability Statement: Not applicable.

Conflicts of Interest: The authors declare no conflict of interest.

References

1. Del Pino-Lopez, J.C.; Cruz-Romero, P. Magnetic field shielding of underground cable duct banks. *Prog. Electromagn. Res.* **2013**, *138*, 1–19.
2. Royal, A.; Atkins, P.; Brennan, M.; Chapman, D.; Chen, H. Site assessment of multiple-sensor approaches for buried utility detection. *Int. J. Geophys.* **2011**, *2011*, 496123.
3. Khoroshev, A.S.; Gummel', A.A.; Kosarev, A.S. Estimating Possibility of Applying Magnetic Sensors in Advanced Probing System of Tunneling Shield. In Proceedings of the International Russian Automation Conference (RusAutoCon), Sochi, Russia, 9–16 September 2018; pp. 1–4.
4. Zhivodernikov, A.V.; Pavlenko, A.V.; Puzin, V.S. Numerical and Experimental Study of a Device for Electrical Power Lines Probing for a Tunnel-Boring Complex Control System. *Machines* **2021**, *9*, 35. <https://doi.org/10.3390/machines9020035>.
5. Khoroshev, A.S.; Vasyukov, I.V.; Zemlyanoy, S.A. Experimental Investigation of Possible Use of Ferroprobe Sensors in Advanced Exploration System of Tunneling Shield. In Proceedings of the 2019 International Russian Automation Conference (RusAutoCon), Sochi, Russia, 8–14 September 2019.
6. Khoroshev, A.S.; Zhivodernikov, A.V.; Kosarev, A.S. Performance Evaluation of the Magnetic Sensored System of Electrical Communications Advanced Probing for a Micro-Tunnel-Boring Shield in a Weakened Electromagnetic Field. In Proceedings of the 2020 International Russian Automation Conference (RusAutoCon), Sochi, Russia, 6–12 September 2020.
7. Geuzaine, C.; Remacle, J.-F. Gmsh: A three-dimensional finite element mesh generator with built-in pre- and post-processing facilities. *Int. J. Numer. Methods Eng.* **2009**, *79*, 1309–1331.
8. Rebay, S. Efficient unstructured mesh generation by means of Delaunay triangulation and Bowyer-Watson algorithm. *J. Comput. Phys.* **1993**, *106*, 125–138.
9. Khoroshev, A.; Pavlenko, A.; Batishchev, D.; Puzin, V. Verification program complex GMSH + GETDP for finite element modeling of electromagnetic fields. Proceedings of the higher educational institutions. North Caucasian region. *Ser. Eng. Sci.* **2013**, *6*, 74–78.
10. Biro, O. Edge element formulations of eddy current problems. *Comput. Methods Appl. Mech. Eng.* **1999**, *169*, 391–405.
11. Biro, O.; Paul, C.; Preis, K. "The use of a reduced vector potential A-r formulation for the calculation of iron induced field errors", ROXIE: Routine for the Optimization of Magnet X-Sections, Inverse Field Calculation and Coil End Design. In Proceedings of the First International Roxie Users Meeting and Workshop CERN, 16–18 March 1998, Geneva, Switzerland; pp. 31–47.
12. Geuzaine, C. High Order Hybrid Finite Element Schemes for Maxwell Equations Taking Thin Structures and Global Quantities into Account. Ph.D. Thesis, Université de Liège, Liège, Belgium, 2001; 174p, pp. 71–80.
13. Dular, P.; Geuzaine, C.; Henrotte, F. A general environment for the treatment of discrete problems and its application to the finite element method. *IEEE Trans. Magn.* **1998**, *34*, 3395–3398.
14. Dular, P.; Geuzaine, C.; Genon, A.; Legros, W. An evolutive software environment for teaching finite element methods in electromagnetism. *IEEE Trans. Magn.* **1999**, *35*, 1682–1685.
15. Albanese, R.; Rubinacci, G. Magnetostatic field computations in terms of two-component vector potentials. *Int. J. Numer. Meth. Engng.* **1990**, *29*, 515–532.
16. Manges, J.B.; Cendes, Z.J. A generalized tree-cotree gauge for magnetic field computation. *IEEE Trans. Magn.* **1995**, *31*, 1342–1347.
17. Creusé, E.; Dular, P.; Nicaise, S. About the gauge conditions arising in Finite Element magnetostatic problems. *Comput. Math. Appl.* **2019**, *77*, 1563–1582.
18. Balay, S.; Abhyankar, S.; Adams, M.F.; Adams, M.-F.; Benson, S.; Brown, J.; Brune, P.; Buschelman, K.; Constantinescu, E.-M.; Dalcin, L.; Dener, A.; et al. PETSc Web Page. 2020. Available online: <http://www.mcs.anl.gov/petsc> (accessed on 1 November 2022).
19. Gregoire, R. *Coupling MUMPS and Ordering Software*; CERF ACS Report; WN/PA/02/24; CERFAC: Toulouse, France, 2002.
20. AMD. BLAS-like Library Instantiation Software Framework. Available online: <https://github.com/amd/blis> (accessed on 1 November 2022).
21. Karypis, G.; Kumar, V. METIS—A Software Package for Partitioning Unstructured Graphs, Partitioning Meshes and Computing Fill-Reducing Ordering of Sparse Matrices. 1997. Available online: <https://hdl.handle.net/11299/215346> (accessed on 1 November 2022).
22. Field Density Sensor HB0391.5-20/3. Magnitnye Prybory LLC. Solutions for Instruments of Permanent and Variable Magnetic Fields Monitoring, 2017–2018. Available online: <http://www.magnetic.spb.ru/products/31125218> (accessed on 1 November 2022).